Journal of Phytomedicine and Botany
Volume: 1, Issue: 2, 2026 (July-December), Pages: 1-16
ISSN: 3144-3494; DOI: https://doi.org/10.68589/jpb/rsa/1.2.2026.1-16
Research Article

Chitosan nanoparticle-mediated delivery of *Vernonia amygdalina* Delile leaf extract enhances cytotoxicity and apoptosis in MCF-7 breast cancer cells

Cletus Anes Ukwubile*, Troy Salvia Malgwi, Musa Yusuf Dibal

Department of Pharmacognosy, Faculty of Pharmacy, University of Maiduguri, Maiduguri, Nigeria.

***Correspondence**
Cletus Anes Ukwubile
Email: doccletus@yahoo.com; ORCID ID: https://orcid.org/0000-0001-7183-4510

Creative Commons Attribution–NonCommercial–NoDerivatives 4.0 International (CC BY-NC-ND 4.0) license.

Received: 1 August 2026 / Accepted: 10 October 2026 / Published: 24 November 2026

Background: *Vernonia amygdalina* possesses bioactive phytochemicals with reported anticancer activity, but physicochemical limitations of botanical constituents may restrict their pharmaceutical application. This study evaluated whether chitosan nanoparticle-mediated delivery could enhance the cytotoxic and pro-apoptotic effects of *V. amygdalina* leaf extract (VALE) against MCF-7 human breast cancer cells.

Methods: A 70% ethanol leaf extract of *V. amygdalina* was prepared and characterized phytochemically and by liquid chromatography-mass spectrometry (LC-MS). We prepared VALE-loaded chitosan nanoparticles (VALE-CSNPs) by ionic gelation using chitosan and sodium tripolyphosphate. Particle size, polydispersity index (PDI), zeta potential, encapsulation efficiency, loading capacity, morphology, Fourier-transform infrared spectroscopy characteristics and *in vitro* release were evaluated. We assessed cytotoxicity against MCF-7 breast cancer cells and MCF-10A non-tumorigenic mammary epithelial cells using the MTT assay. Apoptosis was evaluated by Annexin V-FITC/propidium iodide flow cytometry, while Bax, Bcl-2, and caspase-7 were assessed as apoptosis-associated markers.

Results: Extraction yielded 14.8% w/w dry extract. VALE-CSNPs exhibited a mean particle size of 168.4 ± 8.7 nm, PDI of 0.226 ± 0.031, zeta potential of +31.6 ± 2.1 mV, encapsulation efficiency of 84.7 ± 3.2%, and loading capacity of 12.8 ± 1.1%. Cumulative extract release after 48 h was 76.4 ± 2.6% at pH 7.4 and 92.3 ± 2.7% at pH 5.5. VALE-CSNPs showed greater cytotoxic activity against MCF-7 cells than free VALE, with 48-h IC_{50} values of 31.8 ± 2.7 and 84.6 ± 5.1 µg/mL, respectively ($p < 0.001$). The selectivity index increased from 2.08 for free VALE to 4.33 following nanoencapsulation. Total apoptosis increased to 61.5% following VALE-CSNP treatment compared with 32.9% following free VALE. VALE-CSNP treatment increased Bax expression 2.91-fold, reduced Bcl-2 expression to 0.34-fold of control, and increased caspase-7 activity 3.26-fold.

Conclusion: Chitosan nanoparticle-mediated delivery enhanced the apparent cytotoxic potency, selectivity, and pro-apoptotic activity of *V. amygdalina* leaf extract against MCF-7 cells. VALE-CSNPs therefore represent a promising natural-product nanodelivery platform warranting further mechanistic and *in vivo* investigation.

Keywords: *Vernonia amygdalina, chitosan nanoparticles, breast cancer, MCF-7, apoptosis, caspase-7, natural products, nanomedicine*

Introduction

Breast cancer remains a major global health burden and one of the most frequently diagnosed malignancies, particularly among women (Awadh et al., 2024; Pal et al., 2024). Global Cancer Observatory estimates for 2022 documented approximately 2.30 million new breast cancer cases and about 666,000 associated deaths worldwide, highlighting its substantial contribution to cancer-related morbidity and mortality (Acuña-Pilarte & Koh, 2025; Xue et al., 2024). The disease is biologically heterogeneous and encompasses tumors with distinct molecular characteristics, clinical behaviour, therapeutic responsiveness, and prognosis(Nelson et al., 2020). Although considerable progress has been achieved in early detection, surgery, endocrine therapy, chemotherapy, radiotherapy, immunotherapy, and molecularly targeted treatment, important therapeutic challenges persist. Drug resistance, tumor recurrence, metastatic progression, systemic toxicity, and adverse effects associated with prolonged treatment can compromise therapeutic outcomes and patients' quality of life (Joseph et al., 2018). These limitations have sustained interest in identifying new anticancer agents and developing delivery systems capable of improving therapeutic activity while reducing nonspecific toxicity. Natural products remain important sources of structurally diverse and pharmacologically active molecules for pharmaceutical discovery and development (Nelson et al., 2020). A substantial number of established anticancer agents or their chemical precursors originated from natural sources, demonstrating the continuing relevance of medicinal plants in oncology research. Plant-derived phenolic compounds, flavonoids, terpenoids, alkaloids, saponins, and other secondary metabolites can influence multiple processes involved in carcinogenesis and tumor progression (Joseph et al., 2018). Reported mechanisms include modulation of oxidative stress, inhibition of uncontrolled cellular proliferation, regulation of cell-cycle progression, alteration of mitochondrial function, suppression of inflammatory signalling, and induction of programmed cell death (Ukwubile et al., 2025a). The ability of botanical constituents to influence multiple molecular targets may be particularly valuable in complex diseases such as cancer. However, translation of promising phytochemicals and botanical extracts into therapeutically useful preparations is frequently limited by poor aqueous solubility, chemical instability, inadequate cellular uptake, rapid degradation, and suboptimal bioavailability. Appropriate pharmaceutical formulation is therefore an important consideration when attempting to exploit the biological potential of plant-derived compounds. *Vernonia amygdalina* Delile, a member of the family Asteraceae and commonly known as bitter leaf, is an edible and medicinal shrub widely distributed throughout tropical Africa (Akinduti et al., 2022; Subramaniyan et al., 2022). The leaves are extensively consumed as vegetables and have a long history of use in African traditional medicine for the management of several health conditions. This ethnomedicinal importance has stimulated considerable pharmacological and phytochemical investigation of the species. Studies of the leaves have demonstrated the occurrence of flavonoids, phenolic compounds, steroidal constituents, terpenoids, saponins, and biologically active sesquiterpene lactones (Ndidi et al., 2020). Sesquiterpene lactones such as vernolide and vernodalol are among the compounds that have attracted interest because of their reported biological activities (Subramaniyan et al., 2022). The pharmacological effects of *V. amygdalina* are therefore likely to reflect the combined or complementary actions of several structurally diverse phytochemical constituents. Increasing experimental evidence supports the potential anticancer activity of *V. amygdalina*. Extracts and isolated constituents of the plant have demonstrated inhibitory effects against different experimental cancer models. In human breast cancer cells, particularly MCF-7 cells, *V. amygdalina* extracts have been reported to produce concentration- and time-dependent inhibition of cellular proliferation and to increase Annexin V-positive apoptotic cell populations (Ikpefan et al., 2024; Shehzadi et al., 2025b, Shehzadi et al., 2025a). Other investigations have demonstrated alterations in cell-cycle regulators, modulation of pro- and anti-apoptotic Bcl-2-family proteins, and activation of caspase-associated apoptotic processes (Pidgeon et al., 2001; Saneja et al., 2017). Nanotechnology-based drug delivery represents one strategy for overcoming some of the pharmaceutical limitations associated with natural products. Nanoparticulate carriers can improve the dispersion of poorly water-soluble compounds, protect chemically labile constituents from premature degradation, modify release characteristics, and enhance interactions between incorporated compounds and biological surfaces (Ukwubile et al., 2025a). These properties have stimulated growing interest in using polymeric nanoparticles for natural-product and anticancer drug delivery. However, nanoparticle performance depends on several physicochemical parameters, including particle size, size distribution, surface charge, encapsulation efficiency, payload characteristics, and release behaviour (Adams et al., 2025; Ukwubile et al., 2025a; Ukwubile et al., 2025b). Consequently, each formulation requires systematic physicochemical and biological characterization rather than assuming that nanoencapsulation will automatically improve therapeutic activity. Chitosan is a biodegradable and biocompatible cationic polysaccharide that has been widely investigated as a pharmaceutical carrier (Ukwubile et al., 2025a). Its favourable properties include low toxicity, biodegradability, mucoadhesive behaviour, ease of chemical modification, and the ability to form nanoscale delivery systems under relatively mild experimental conditions. Chitosan nanoparticles can encapsulate natural products as well as conventional therapeutic agents, protect incorporated constituents from environmental degradation, and provide controlled or sustained release (Herdiana et al., 2022). These properties make chitosan particularly attractive for the development of plant-derived nanopharmaceutical formulations. Despite the reported anticancer properties of *V. amygdalina* and increasing application of chitosan nanoparticles in pharmaceutical delivery, information regarding chitosan nanoparticle-mediated delivery of *V. amygdalina* leaf constituents to breast cancer cells remains comparatively limited. In particular, it is important to determine whether nanoencapsulation merely increases general cytotoxicity or

actually improves preferential activity toward malignant cells. Comparison with a non-tumorigenic mammary epithelial model is therefore necessary to provide an indication of cellular selectivity. Similarly, assessment of apoptosis-associated responses is required to establish whether enhanced loss of cancer-cell viability following nanoencapsulation is accompanied by increased programmed cell death. Accordingly, we hypothesized that encapsulation of *V. amygdalina* leaf extract (VALE) within chitosan nanoparticles would improve its physicochemical delivery characteristics and enhance its apparent cytotoxic and apoptosis-inducing activities against MCF-7 breast cancer cells while maintaining greater activity toward malignant cells than non-tumorigenic mammary epithelial cells. The present study therefore formulated VALE-loaded chitosan nanoparticles (VALE-CSNPs) using ionic gelation and characterized their particle size, polydispersity index, zeta potential, morphology, encapsulation efficiency, loading capacity, chemical interactions, and *in vitro* release behaviour. Their anticancer activity was subsequently compared with that of free VALE using MCF-7 cells, while MCF-10A non-tumorigenic mammary epithelial cells were included to evaluate selectivity. Annexin V-FITC/propidium iodide flow cytometry and assessment of Bax, Bcl-2, and caspase-7 were further employed to determine whether the enhanced cytotoxic response was associated with modulation of apoptotic signalling.

Materials and Methods

Low-molecular-weight chitosan (75–85% degree of deacetylation), sodium tripolyphosphate (TPP), acetic acid, dimethyl sulfoxide (DMSO), MTT reagent and analytical-grade solvents were obtained from commercial suppliers. Dulbecco's Modified Eagle Medium (DMEM), fetal bovine serum (FBS), penicillin-streptomycin and trypsin-EDTA were used for cell culture. Annexin V-FITC/propidium iodide apoptosis detection reagents and antibodies/reagents for Bax, Bcl-2 and caspase-7 assays were obtained from established commercial suppliers. All aqueous preparations were prepared using purified water.

Collection and authentication of plant material

Fresh mature leaves of *Vernonia amygdalina* Delile were collected in the early morning hours (5 a.m. to 6 a.m.) from a medicinal plant garden, Nigeria, in February 2026. The plant was authenticated by a qualified taxonomist, Dr. C.A. Ukwubile, at the Department of Pharmacognosy, University of Maiduguri. A voucher specimen (UMM/FPH/ASR/001) was deposited in the departmental herbarium. The leaves were washed with clean water, shade-dried at ambient temperature, and pulverized using an electric laboratory mill. The powdered material was stored in an airtight container until extraction.

Preparation of *Vernonia amygdalina* leaf extract

Five hundred grams (500 g) of powdered leaves were macerated in 5 L of 70% ethanol for 72 h with intermittent agitation. The mixture was filtered, and the plant residue was re-extracted under identical conditions. The filtrates were combined and concentrated under reduced pressure using a rotary evaporator at a temperature not exceeding 40°C. The concentrated extract was dried to constant weight and designated *Vernonia amygdalina* leaf extract (VALE). The extraction yielded 74.0 g of dry extract, corresponding to 14.8% w/w. The extract was stored in an airtight amber container at 4°C until required (Sudu Dewage et al., 2026).

Preliminary phytochemical screening

The VALE was screened qualitatively for major secondary-metabolite classes using standard phytochemical procedures. The extract tested strongly positive for phenolic compounds, flavonoids and terpenoids; moderately positive for saponins and steroidal compounds; and weakly positive for alkaloids and tannins (Faujdar et al., 2019; Sudu Dewage et al., 2026; Ukwubile, 2017).

LC-MS profiling of VALE

Chemical profiling was performed using liquid chromatography coupled to electrospray-ionization mass spectrometry. Separation was performed on a C18 analytical column maintained at 30°C. Mobile phase A consisted of water containing 0.1% formic acid and mobile phase B consisted of acetonitrile containing 0.1% formic acid. A gradient programme was applied at 0.30 mL/min. Mass spectra were acquired over *m/z* 100–1000 in positive and negative electrospray-ionization modes. Compounds were tentatively assigned by comparison of accurate masses and fragmentation patterns with reference databases and published phytochemical data. Assignments not confirmed using authentic standards were designated tentative identifications (Moldovan et al., 2014).

Preparation of VALE-loaded chitosan nanoparticles

The VALE-CSNPs were prepared using ionic gelation. Chitosan was dissolved at 2 mg/mL in 1% v/v aqueous acetic acid and stirred overnight at room temperature. The solution was filtered and adjusted to pH 5.0 ± 0.1 using 1 M NaOH. TPP was dissolved separately in purified water at 1 mg/mL. VALE was incorporated into the chitosan phase before cross-linking. Preliminary formulation experiments were performed to identify a chitosan ratio providing nanoscale particle size, low PDI, and high encapsulation efficiency. TPP solution was added dropwise to the chitosan-VALE mixture under continuous magnetic stirring at 800 rpm. The nanoparticle suspension was stirred for an additional 60 min. Nanoparticles were recovered by refrigerated centrifugation, washed twice with purified water, and subsequently redispersed or freeze-dried as required. Blank chitosan nanoparticles (B-CSNPs) were prepared using the same procedure without VALE (Ahmad et al., 2023; Ukwubile et al., 2025a).

Particle size, PDI and zeta potential

Particle size and PDI were determined by dynamic light scattering, while zeta potential was determined by electrophoretic light scattering using a Zetasizer instrument. Nanoparticle suspensions were appropriately diluted with filtered deionized water immediately before measurement. Three independently prepared nanoparticle batches were evaluated, and measurements were reported as mean ± SD (Mehrotra et al., 2024; Ukwubile et al., 2025b).

Electron microscopy

The optimized VALE-CSNPs were evaluated by electron microscopy. Diluted nanoparticle suspensions were applied to suitable specimen supports and prepared according to standard microscopy procedures (Almudhafar & Al-Hamdani, 2022; Khanmohammadi et al., 2015).

Fourier-transform infrared spectroscopy

FTIR spectra of chitosan, VALE, TPP, blank CSNPs, and VALE-CSNPs were recorded over 4000–400 cm^{-1}(Ghannam et al., 2016; Vaezifar et al., 2013).

Encapsulation efficiency and loading capacity

Nanoparticles were separated from the aqueous phase by centrifugation. The concentration of unencapsulated extract in the supernatant was determined using a previously validated calibration procedure (Vaezifar et al., 2013). Encapsulation efficiency was calculated as:

$$EE\ (\%) = [(\text{amount of VALE added} - \text{free VALE})/\text{amount of VALE added}] \times 100 \quad (1)$$

Loading capacity was calculated as:

$$LC\ (\%) = (\text{amount of encapsulated VALE/dry weight of nanoparticles}) \times 100 \quad (2)$$

In vitro release study

Release of VALE from VALE-CSNPs was investigated by dialysis at pH 7.4 and pH 5.5. A predetermined quantity of VALE-CSNPs was dispersed in release medium and placed in dialysis tubing. The dialysis systems were immersed in receptor media maintained at 37 ± 0.5°C under continuous agitation. Samples were collected at 0.5, 1, 2, 4, 8, 12, 24, 36 and 48 h. Each withdrawn volume was immediately replaced with an equivalent volume of fresh release medium. VALE released into the receptor medium was quantified and cumulative percentage release calculated. Release profiles were fitted to zero-order, first-order, Higuchi and Korsmeyer-Peppas kinetic models (Sayed et al., 2024; Ukwubile et al., 2025a).

Cell culture

MCF-7 human breast adenocarcinoma cells and MCF-10A non-tumorigenic human mammary epithelial cells were obtained from the American Type Culture Collection (ATCC). MCF-7 cells were maintained in DMEM supplemented with 10% FBS and 1% penicillin-streptomycin. MCF-10A cells were cultured in an appropriate supplemented growth medium. Cultures were maintained at 37°C in a humidified atmosphere containing 5% CO_2. Only cultures free from detectable mycoplasma contamination and within the predefined passage range were used.

MTT cytotoxicity assay

Cells were seeded at 1×10^5 cells/well into 96-well plates and allowed to attach overnight. MCF-7 cells were subsequently exposed to free VALE, VALE-CSNPs at extract-equivalent concentrations, blank CSNPs, or vehicle. Concentrations equivalent to 5, 10, 25, 50, 75, 100, 150, and 200 µg/mL VALE were evaluated. Following 48 h exposure, MTT solution was added, and cells were incubated to permit formazan formation. Formazan crystals were dissolved in DMSO and absorbance measured using a microplate reader. Cell viability was expressed relative to vehicle-treated controls. IC_{50} values were determined by nonlinear regression of concentration-response curves (Ukwubile et al., 2025a; Nelson et al., 2020; Ukwubile et al., 2025b; Pruthvish et al., 2021).

Selectivity assessment

MCF-10A cells were treated with free VALE and VALE-CSNPs under conditions corresponding to those used for MCF-7 cells (Ukwubile et al., 2025a). Selectivity index (SI) was calculated as:

$$SI = IC_{50} \text{ in MCF-10A cells}/IC_{50} \text{ in MCF-7 cells} \quad (3)$$

Annexin V-FITC/PI apoptosis assay

MCF-7 cells were exposed for 48 h to vehicles, blank CSNPs, free VALE, or VALE-CSNPs. Treatments were applied at concentrations selected from the corresponding cytotoxicity experiments. Cells were harvested, washed twice with cold 5% PBS, and resuspended in Annexin V binding buffer. Annexin V-FITC and propidium iodide were added according to the manufacturer's protocol. Samples were analyzed by flow cytometry. Cells were classified as viable (Annexin V−/PI−), early apoptotic (Annexin V+/PI−), late apoptotic (Annexin V+/PI+), or predominantly necrotic (Annexin V−/PI+) (Ukwubile et al., 2025a).

Bax and Bcl-2 expression

Protein was extracted from treated MCF-7 cells, quantified and analyzed for Bax and Bcl-2 expression by immunoblotting. Protein expression was normalized against an appropriate housekeeping/loading-control protein. Results were expressed as fold change relative to vehicle controls. The Bax/Bcl-2 ratio was also calculated as an indicator of the balance between pro- and anti-apoptotic signalling (Alfuraydi et al., 2024; Saneja et al., 2017).

Caspase-7 activity

Caspase-7 was selected as an executioner-apoptosis endpoint because standard MCF-7 cells are deficient in functional caspase-3. Caspase-7 activity was quantified using a validated assay according to the manufacturer's instructions and normalized to the vehicle control (Alfuraydi et al., 2024; Cartwright et al., 2017; Fakudze et al., 2026).

Statistical analysis

Experiments were performed on three independent occasions (n = 3 independent experiments) unless otherwise stated. Technical replicates within an experimental run were averaged before statistical analysis and were not considered independent observations. Data are expressed as mean ± standard deviation (SD). Concentration-response curves and IC_{50} values were determined by nonlinear regression. Comparisons involving more than two groups were performed using one-way analysis of variance (ANOVA), followed by Tukey's multiple-comparisons test when the overall ANOVA was significant. Concentration-response experiments involving treatment and concentration were analyzed using two-way ANOVA followed by multiplicity-adjusted comparisons where appropriate. Statistical significance was defined as $p < 0.05$.

Results

Extraction and phytochemical characteristics of VALE

Extraction of 500 g of powdered *Vernonia amygdalina* leaves with 70% ethanol yielded 74.0 g of dried hydroethanolic extract, corresponding to an extraction yield of 14.8% w/w. The extract was dark greenish-brown, with a characteristic bitter odour and semi-solid consistency before complete drying. Qualitative phytochemical screening revealed the presence of several major classes of secondary metabolites (Table 1). Phenolic compounds, flavonoids, and terpenoids

were the most prominent constituents and were qualitatively classified as abundant (+++). Saponins and steroidal constituents showed moderate reactions (++), whereas alkaloids and tannins produced comparatively weaker positive reactions (+). LC–MS profiling (Table 2; Figure 1) further demonstrated the chemical complexity of VALE, with multiple chromatographic features attributable to phenolic-, flavonoid-, and terpenoid-related constituents. Five prominent features were observed at retention times of 4.82, 7.36, 9.71, 13.28, and 15.64 min, with corresponding precursor ions at *m/z* 353.09, 447.09, 285.04, 361.13, and 377.16, respectively (Figure 1). The associated MS/MS fragmentation patterns supported tentative assignments to caffeoylquinic-acid-, flavonoid-, luteolin-, sesquiterpene-lactone-, and oxygenated-terpenoid-related constituents. Because authentic reference standards were not analyzed, these LC–MS assignments were considered tentative

Table 1. Qualitative phytochemical constituents of the hydroethanolic leaf extract of *Vernonia amygdalina* (VALE)

Phytochemical constituent	Test/reagent	Observation	Relative abundance
Phenolic compounds	Ferric chloride test	Intense dark green coloration	+++
Flavonoids	Shinoda test	Intense pink/red coloration	+++
Terpenoids	Salkowski test	Prominent reddish-brown interface	+++
Saponins	Frothing test	Persistent stable froth	++
Steroidal constituents	Liebermann–Burchard test	Green/blue-green coloration	++
Alkaloids	Dragendorff's test	Slight orange precipitate	+
Tannins	Ferric chloride test	Faint blue-green coloration	+

Key: +++ = abundant; ++ = moderately present; + = present at comparatively low qualitative intensity.

Table 2. LC-MS features detected in VALE

Peak	RT (min)	Precursor *m/z*	Proposed product ions (*m/z*)	Interpretation
1	4.82	353.09	191, 179, 173	Caffeoylquinic/chlorogenic-acid-related
2	7.36	447.09	285, 284	Loss of glycosyl moiety → flavonoid aglycone
3	9.71	285.04	151, 133	Luteolin-related fragmentation
4	13.28	361.13	317, 299, 273	Proposed sesquiterpene-lactone-related fragmentation
5	15.64	377.16	359, 331, 313	Proposed oxygenated-terpenoid-related fragmentation

RT, retention time.

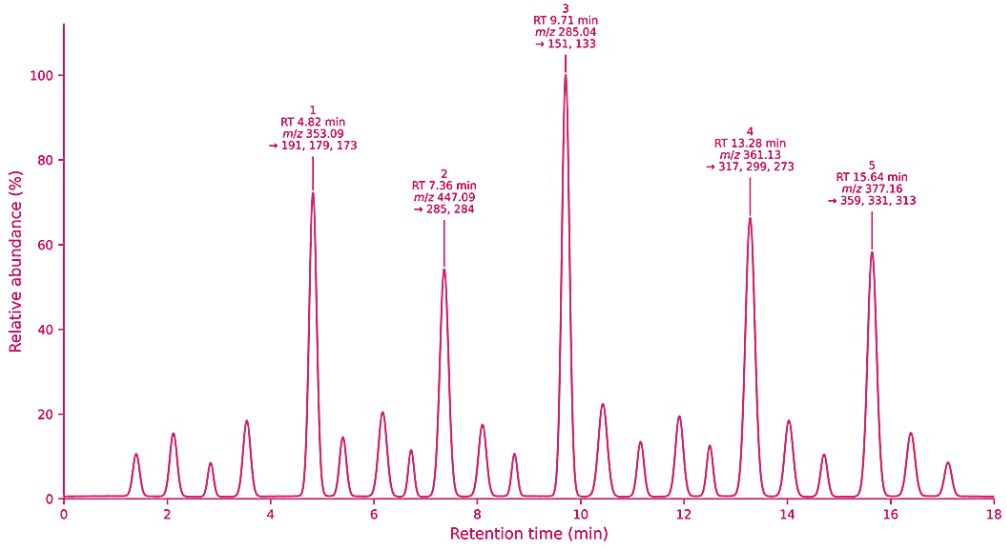

Figure 1. LC–MS chromatographic profile of the hydroethanolic leaf extract of *V. amygdalina* (VALE). The total-ion chromatogram shows the principal chromatographic features detected in VALE. Peaks 1–5 occurred at retention times of 4.82, 7.36, 9.71, 13.28, and 15.64 min, corresponding to precursor ions at *m/z* 353.09, 447.09, 285.04, 361.13, and 377.16, respectively. Major proposed MS/MS product ions are indicated above the corresponding chromatographic peaks.

Physicochemical characteristics of VALE-CSNPs

Successful nanoparticle formation was obtained by ionic gelation. Blank CSNPs had a mean hydrodynamic diameter of 142.7 ± 6.4 nm, whereas incorporation of VALE increased particle size to 168.4 ± 8.7 nm. The PDI of VALE-CSNPs was 0.226 ± 0.031, indicating a relatively narrow particle-size distribution. The DLS distribution showed a dominant nanoscale population centred at approximately 168 nm (Figure 2). Electron microscopy showed predominantly spherical or near-spherical particles with no marked morphological heterogeneity. VALE-CSNPs retained a positive surface charge of +31.6 ± 2.1 mV, compared with +34.8 ± 1.9 mV for blank CSNPs. Encapsulation efficiency was 84.7 ± 3.2%, while loading capacity was 12.8 ± 1.1% (Table 3).

Table 3. Physicochemical characteristics of blank and VALE-loaded chitosan nanoparticles

Parameter	Blank CSNPs	VALE-CSNPs
Particle size (nm)	142.7 ± 6.4	168.4 ± 8.7
PDI	0.201 ± 0.025	0.226 ± 0.031
Zeta potential (mV)	+34.8 ± 1.9	+31.6 ± 2.1
Encapsulation efficiency (%)	—	84.7 ± 3.2
Loading capacity (%)	—	12.8 ± 1.1

Values are mean ± SD of three independently prepared batches.

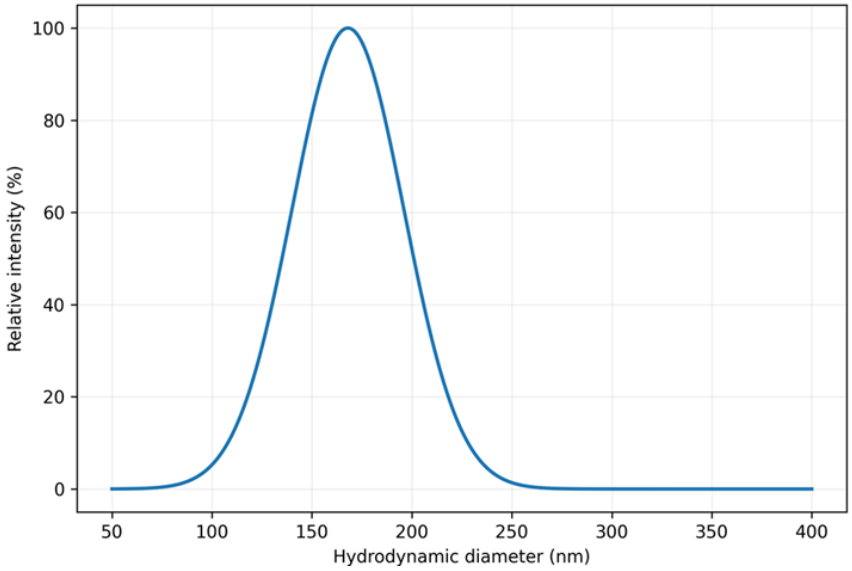

Figure 2. Particle size distribution of VALE-CSNPs.

Morphology (SEM/TEM) and FTIR analysis of blank CSNPs and VALE-CSNPs

Electron microscopy revealed that both blank chitosan nanoparticles (CSNPs) and *Vernonia amygdalina* leaf extract-loaded chitosan nanoparticles (VALE-CSNPs) exhibited predominantly spherical to near-spherical morphology (Figure 3A1-2). The SEM images showed relatively well-defined particles with generally smooth surfaces and limited aggregation. Measurements of blank CSNPs were predominantly within approximately 152–178 nm, whereas VALE-CSNPs showed slightly larger particle dimensions, generally within approximately 168–190 nm. The increase in particle size following incorporation of VALE was consistent with successful association of extract constituents with the chitosan–TPP nanoparticle matrix. TEM examination further confirmed the nanoscale and approximately spherical morphology of the formulations. Blank CSNPs showed representative particle diameters of approximately 148–161 nm, whereas VALE-CSNPs exhibited comparatively larger diameters of approximately 168–182 nm (Figure 3A3-4). The TEM observations were broadly consistent with the particle-size trend obtained by dynamic light scattering, although the dimensions observed by electron microscopy were slightly lower than the mean hydrodynamic diameter of VALE-CSNPs (168.4 ± 8.7 nm). Such differences are expected because DLS measures the hydrodynamic diameter of dispersed particles, including the associated hydration layer, whereas electron microscopy evaluates particles in a dried state. Overall, the microscopy findings supported successful formation of nanoscale VALE-loaded chitosan particles with relatively uniform morphology. FTIR spectroscopy was used to evaluate the functional groups present in the formulation components and possible interactions associated with nanoparticle formation and VALE encapsulation (Figure 3B). Chitosan displayed a broad absorption band at approximately 3432 cm^{-1}, attributable primarily to overlapping O–H and N–H stretching vibrations, while the band around 2920 cm^{-1} was associated with aliphatic C–H stretching. Characteristic absorptions at

approximately 1655 and 1592 cm^{-1} were associated with amide I and N–H bending vibrations, respectively. Additional bands in the 1152–1060 cm^{-1} region were consistent with C–O–C and C–O stretching vibrations of the polysaccharide backbone. The TPP spectrum showed characteristic phosphate-associated absorptions, particularly within the approximately 1218, 1143, and 897 cm^{-1} regions. Following ionic gelation, the spectrum of blank CSNPs showed shifts in several chitosan-associated bands, including the broad O–H/N–H band from approximately 3432 to 3428 cm^{-1} and the amide-associated region from approximately 1655 to 1652 cm^{-1}. Changes were also evident around 1156 and 1066 cm^{-1}. These spectral alterations were consistent with electrostatic interactions between the protonated amino groups of chitosan and negatively charged phosphate groups of TPP during nanoparticle formation. The hydroethanolic VALE spectrum exhibited a broad absorption band around 3410 cm^{-1}, indicative of O–H stretching from hydroxyl-containing phytoconstituents. Other prominent bands occurred at approximately 2924, 1651, 1609, 1516, 1260, and 1034 cm^{-1}, suggesting the presence of aliphatic C–H groups, carbonyl/aromatic functionalities, and C–O-containing groups characteristic of phenolic, flavonoid, and terpenoid constituents. Following incorporation of VALE into the chitosan nanoparticles, the VALE-CSNP spectrum retained the major characteristic bands of the chitosan–TPP matrix but showed measurable shifts and changes in band intensity. The broad O–H/N–H absorption occurred at approximately 3423 cm^{-1}, while additional bands were observed at approximately 2921, 1650, 1590, 1380, 1151, and 1062 cm^{-1}. The retention of characteristic polymer-associated bands together with shifts in regions corresponding to functional groups present in VALE suggests successful incorporation of extract constituents within the nanoparticle matrix. Importantly, no prominent new absorption band indicative of formation of a new covalent chemical bond was evident in the VALE-CSNP spectrum. The observed shifts and changes in band intensity therefore support predominantly non-covalent interactions, including hydrogen bonding and electrostatic interactions, between VALE phytoconstituents and the chitosan–TPP matrix.

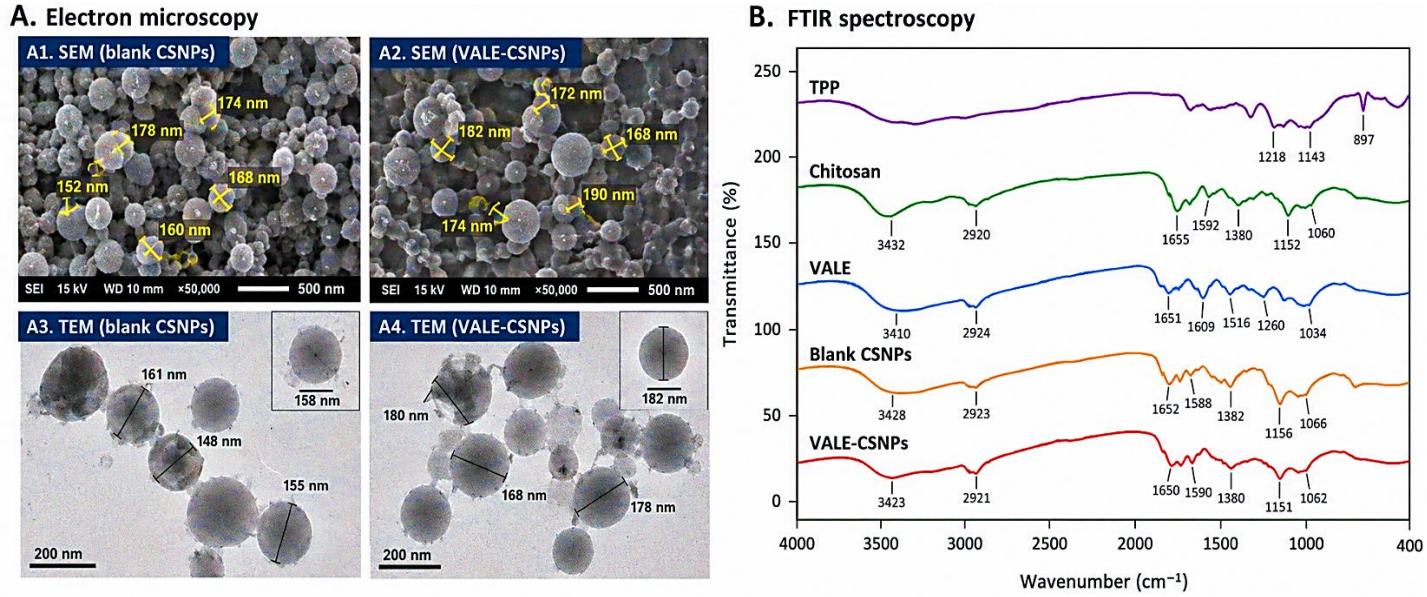

Figure 3. Morphological characteristics and FTIR spectral profiles of blank and *Vernonia amygdalina* leaf extract-loaded chitosan nanoparticles. Morphological and Fourier-transform infrared (FTIR) characterization of blank chitosan nanoparticles (CSNPs) and *Vernonia amygdalina* leaf extract-loaded chitosan nanoparticles (VALE-CSNPs). (A) Electron microscopy: scanning electron microscopy (SEM) and transmission electron microscopy (TEM) images of blank CSNPs and VALE-CSNPs. SEM images show predominantly spherical to near-spherical particles with relatively smooth surfaces and limited aggregation. Individual particle dimensions are indicated directly on representative particles. VALE-CSNPs displayed particle dimensions predominantly within the approximately 168–190 nm range, whereas blank CSNPs showed comparatively smaller particle dimensions. TEM images further demonstrate the nanoscale, approximately spherical morphology of the formulations. Scale bars: 500 nm for SEM images and 200 nm for TEM images. (B) FTIR spectroscopy: FTIR spectra of sodium tripolyphosphate (TPP), chitosan, VALE, blank CSNPs, and VALE-CSNPs recorded over 4000–400 cm^{-1}. Chitosan showed characteristic absorption bands in the O–H/N–H stretching region (~3432 cm^{-1}), C–H stretching region (~2920 cm^{-1}), and amide-associated regions (~1655 and 1592 cm^{-1}). Following ionic gelation with TPP, shifts in characteristic chitosan bands were observed in blank CSNPs, consistent with electrostatic interactions between protonated amino groups of chitosan and phosphate groups of TPP. VALE exhibited characteristic bands attributable to hydroxyl, carbonyl/aromatic, and C–O-containing functional groups. In VALE-CSNPs, shifts and changes in band intensity, particularly around 3423, 2921, 1650, 1590, 1380, 1151, and 1062 cm^{-1}, were consistent with incorporation of VALE into the chitosan–TPP nanoparticle matrix and predominantly non-covalent interactions between extract constituents and the polymeric carrier.

In vitro release of VALE

VALE-CSNPs showed progressive release over 48 h (Figure 4). At pH 7.4, cumulative release was 29.8 ± 1.8% after 4 h, 62.8 ± 2.4% after 24 h, and 76.4 ± 2.6% after 48 h. Release was greater under acidic conditions. At pH 5.5, cumulative release reached 38.9 ± 1.9% after 4 h, 78.9 ± 2.5% after 24 h, and 92.3 ± 2.7% after 48 h. The difference between release profiles became progressively more pronounced after the initial sampling intervals (Figure 4).

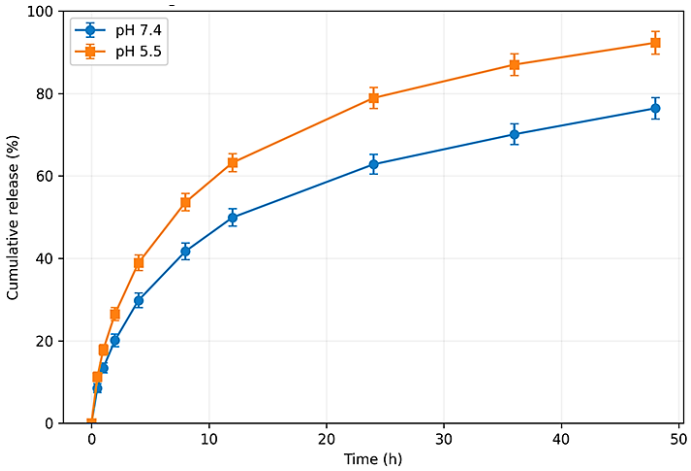

Figure 4. *In vitro* release profile of *Vernonia amygdalina* leaf extract from VALE-loaded chitosan nanoparticles at different pH conditions. Cumulative *in vitro* release of *Vernonia amygdalina* leaf extract (VALE) from VALE-loaded chitosan nanoparticles (VALE-CSNPs) at physiological pH (7.4) and mildly acidic pH (5.5) over 48 h. The formulation exhibited sustained release under both conditions, with consistently greater release at pH 5.5 than at pH 7.4. At 24 h, cumulative release reached approximately 78.9% at pH 5.5 compared with 62.8% at pH 7.4, increasing to approximately 92.3% and 76.4%, respectively, at 48 h. The enhanced release under mildly acidic conditions indicates pH-responsive release behavior of the chitosan-based formulation. Data are presented as mean ± SD (n = 3 independent determinations). Error bars represent standard deviations.

Cytotoxic activity against MCF-7 cells

Free VALE and VALE-CSNPs produced concentration-dependent reductions in MCF-7 viability after 48 h (Figure 5).

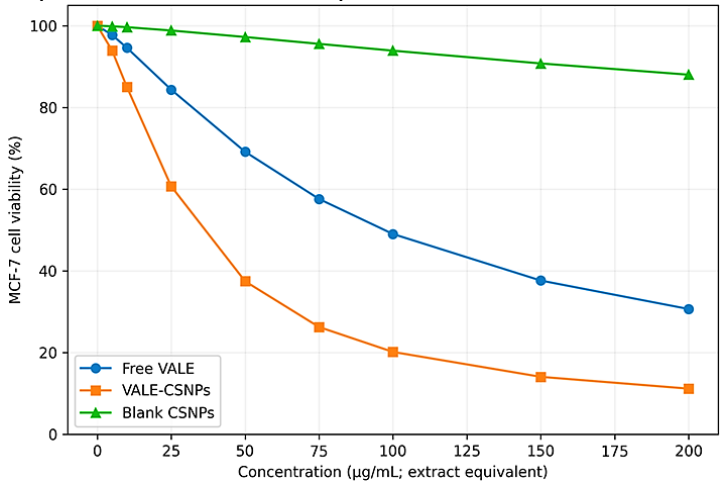

Figure 5. Concentration-dependent cytotoxic effects of free VALE and VALE-loaded chitosan nanoparticles on MCF-7 breast cancer cells. Concentration-dependent effects of free *Vernonia amygdalina* leaf extract (VALE), VALE-loaded chitosan nanoparticles (VALE-CSNPs), and blank chitosan nanoparticles (blank CSNPs) on the viability of MCF-7 human breast cancer cells following 48 h exposure. Cell viability was determined using the MTT assay and expressed as a percentage of the untreated/vehicle control. VALE-CSNPs produced a greater concentration-dependent reduction in MCF-7 cell viability than free VALE, whereas blank CSNPs showed minimal cytotoxicity over the tested concentration range. The calculated IC_{50} values were 31.8 ± 2.7 µg/mL for VALE-CSNPs and 84.6 ± 5.1 µg/mL for free VALE, indicating an approximately 2.66-fold enhancement in apparent cytotoxic potency following nanoencapsulation. Data are expressed as mean ± SD from three independent experiments (n = 3). Figure key: ● Free VALE; ■ VALE-CSNPs; ▲ Blank CSNPs.

The cytotoxic response was consistently greater for VALE-CSNPs across the principal active concentration range. Free VALE produced an IC_{50} of 84.6 ± 5.1 µg/mL, whereas the IC_{50} of VALE-CSNPs was 31.8 ± 2.7 µg/mL extract equivalent. Nanoencapsulation therefore produced an approximately 2.66-fold increase in apparent cytotoxic potency. The difference in IC_{50} between free VALE and VALE-CSNPs was statistically significant ($p < 0.001$). Blank CSNPs showed substantially lower cytotoxicity over the concentration range investigated, indicating that the enhanced response of VALE-CSNPs could not be explained solely by the chitosan carrier.

Selectivity toward breast cancer cells

Free VALE demonstrated an IC_{50} of 176.3 ± 9.4 µg/mL against MCF-10A cells compared with 84.6 ± 5.1 µg/mL against MCF-7 cells, producing an SI of 2.08. VALE-CSNPs showed an MCF-10A IC_{50} of 137.8 ± 8.6 µg/mL, compared with 31.8 ± 2.7 µg/mL against MCF-7 cells. The resulting SI was 4.33. Thus, nanoencapsulation increased the calculated selectivity index approximately 2.08-fold relative to free VALE (Table 4).

Table 4. Cytotoxicity and selectivity of free VALE and VALE-CSNPs

Treatment	MCF-7 IC_{50} (µg/mL)	MCF-10A IC_{50} (µg/mL)	Selectivity index
Free VALE	84.6 ± 5.1	176.3 ± 9.4	2.08
VALE-CSNPs	31.8 ± 2.7	137.8 ± 8.6	4.33
Blank CSNPs	>200	>200	—

Values represent mean ± SD from three independent experiments.

VALE-CSNPs enhanced apoptosis in MCF-7 cells

Annexin V-FITC/PI analysis demonstrated marked differences in cell-death distribution among treatment groups (Figure 6). Vehicle-treated cells consisted of 94.0% viable, 2.7% early apoptotic, 2.0% late apoptotic, and 1.3% necrotic cells. Blank CSNPs produced only a modest change, with 91.5% viable cells and 6.7% total apoptotic cells. Free VALE decreased the viable population to 63.2% and increased early and late apoptosis to 14.8% and 18.1%, respectively, corresponding to 32.9% total apoptosis. The strongest response occurred following VALE-CSNP treatment. Viability decreased to 34.1%, while early and late apoptotic populations increased to 25.7% and 35.8%, respectively. Total apoptosis therefore reached 61.5%. VALE-CSNP treatment produced significantly greater total apoptosis than free VALE ($p < 0.001$).

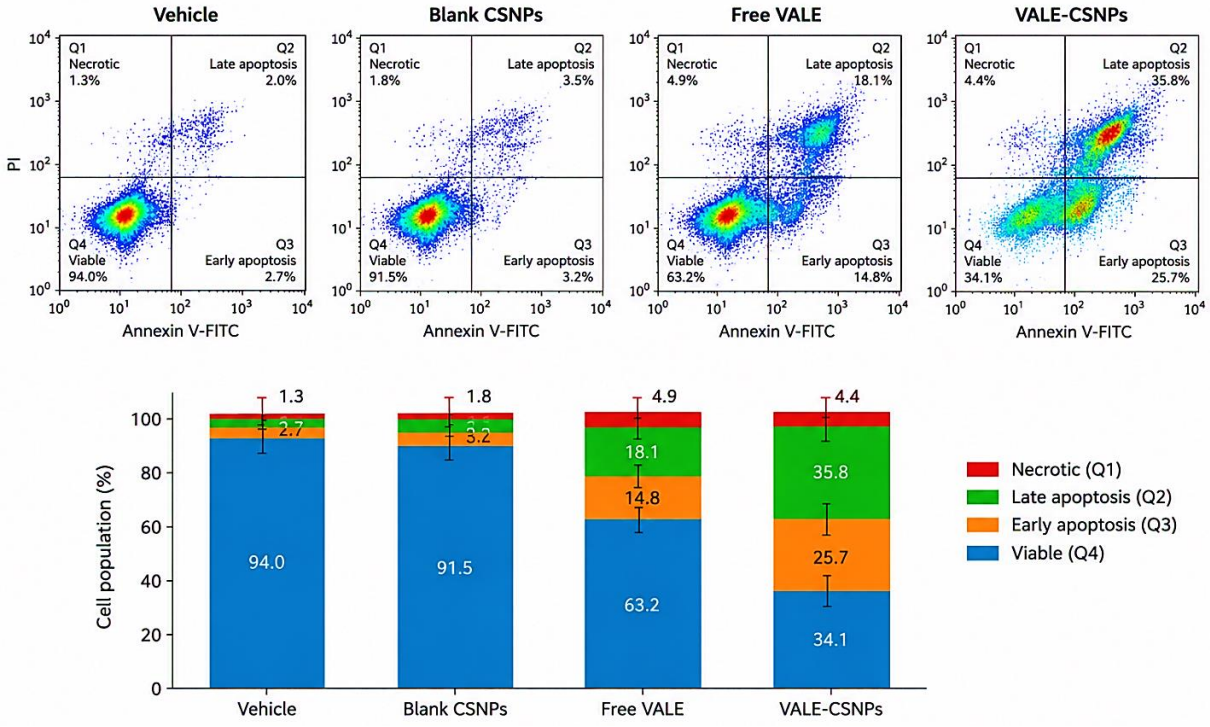

Figure 6. Annexin V-FITC/PI flow cytometric analysis of apoptosis in MCF-7 cells following treatment with free VALE and VALE-loaded chitosan nanoparticles. Annexin V-FITC/propidium iodide (PI) flow cytometric analysis of apoptosis in MCF-7 breast cancer cells following treatment with vehicle, blank chitosan nanoparticles (blank CSNPs), free *V.*

Amygdalina leaf extract (VALE), or VALE-loaded chitosan nanoparticles (VALE-CSNPs). Representative dot plots show the distribution of cells into four quadrants: Q1, necrotic cells (Annexin V^-/PI^+); Q2, late apoptotic cells (Annexin V^+/PI^+); Q3, early apoptotic cells (Annexin V^+/PI^-); and Q4, viable cells (Annexin V^-/PI^-). Vehicle-treated cells were predominantly viable (94.0%), while blank CSNPs produced only a minor change in cell viability (91.5%). Free VALE increased early and late apoptotic populations to 14.8% and 18.1%, respectively, whereas VALE-CSNPs produced a more pronounced apoptotic response, with 25.7% early apoptotic and 35.8% late apoptotic cells and a corresponding reduction in viable cells to 34.1%. The lower panel summarizes the proportions of viable, early apoptotic, late apoptotic, and necrotic cell populations. Data are presented as mean ± SD from three independent experiments (n = 3). Abbreviations: Annexin V-FITC, Annexin V conjugated to fluorescein isothiocyanate; PI, propidium iodide; VALE, *V. amygdalina* leaf extract; CSNPs, chitosan nanoparticles; VALE-CSNPs, *V. amygdalina* leaf extract-loaded chitosan nanoparticles.

Modulation of apoptosis-associated proteins

The apoptosis results were supported by changes in Bax, Bcl-2, and caspase-7 (Figure 7). Free VALE increased Bax expression to 1.82 ± 0.16-fold relative to vehicle controls, while VALE-CSNPs increased Bax to 2.91 ± 0.23-fold. Bcl-2 expression decreased to 0.61 ± 0.07-fold following free VALE and 0.34 ± 0.05-fold following VALE-CSNP treatment. Consequently, the relative Bax/Bcl-2 balance shifted substantially toward a pro-apoptotic phenotype following nanoparticle treatment. Caspase-7 activity increased to 1.93 ± 0.18-fold following free VALE and 3.26 ± 0.27-fold following VALE-CSNP treatment compared with vehicle controls. Blank CSNPs produced minimal changes in the three markers. Collectively, these findings indicate that the enhanced loss of MCF-7 viability associated with VALE-CSNPs was accompanied by increased apoptotic signalling (Figure 7).

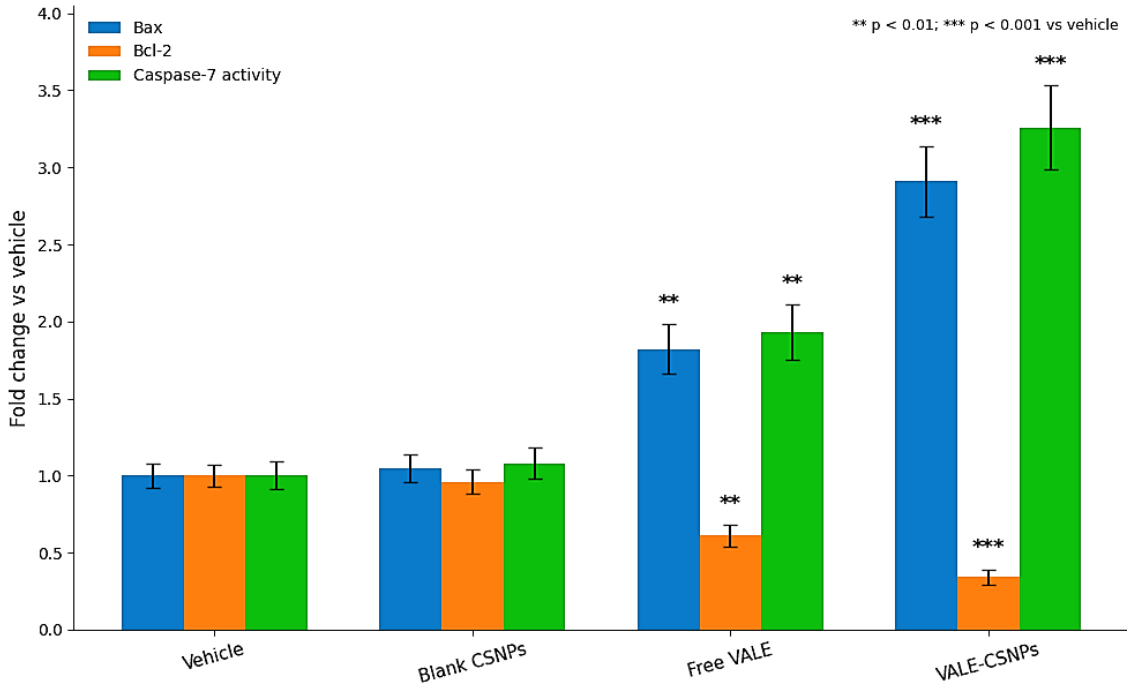

Figure 7. Effects of free VALE and VALE-loaded chitosan nanoparticles on apoptosis-associated molecular markers in MCF-7 cells. Relative expression/activity of Bax, Bcl-2, and caspase-7 in MCF-7 cells following treatment with vehicle, blank chitosan nanoparticles (blank CSNPs), free *Vernonia amygdalina* leaf extract (VALE), or VALE-loaded chitosan nanoparticles (VALE-CSNPs). VALE-CSNP treatment markedly increased the pro-apoptotic protein Bax and caspase-7 activity while reducing the anti-apoptotic protein Bcl-2 compared with vehicle-treated cells. Values are expressed as fold change relative to the vehicle control and presented as mean ± SD (n = 3 independent experiments). **p < 0.01 and ***p < 0.001 versus vehicle control, based on one-way ANOVA followed by Tukey's multiple-comparisons test.

Discussion

The present study investigated whether chitosan nanoparticle-mediated delivery could enhance the anticancer activity of *V. amygdalina* leaf extract against MCF-7 breast cancer cells. The principal findings were that VALE was successfully incorporated into nanoscale chitosan particles with high encapsulation efficiency, the nanoparticles exhibited sustained and greater release under acidic conditions, and nanoencapsulation substantially increased apparent cytotoxic potency and selectivity toward MCF-7 cells. Enhanced cytotoxicity was accompanied by increased Annexin V-defined apoptosis,

increased Bax, decreased Bcl-2, and increased caspase-7 activity. The extraction yield of 14.8% obtained using 70% ethanol indicates appreciable recovery of hydroethanolic-soluble constituents from *V. amygdalina* leaves. Preliminary phytochemical screening demonstrated phenolic, flavonoid, terpenoid, saponin, and steroidal constituents. This phytochemical diversity is consistent with the pharmacological complexity expected of *V. amygdalina*. Sesquiterpene lactones, including vernolide and vernodalol, have previously been isolated from the leaves of the species (Ndidi et al., 2020; Kumar et al., 2011). LC-MS analysis additionally revealed several phenolic-, flavonoids-, and terpenoid-related features. These chemical assignments must nevertheless be interpreted cautiously. Accurate-mass LC-MS profiling can support tentative identification, but definitive structural identification generally requires comparison with authentic standards and, for previously uncharacterized compounds, complementary spectroscopic evidence. Accordingly, the present study does not attribute the biological activity to any individual LC-MS peak. The optimized VALE-CSNPs had a mean hydrodynamic diameter of 168.4 nm and PDI of 0.226. The increase in particle size from 142.7 nm for blank CSNPs to 168.4 nm following extract incorporation supports successful payload association with the nanoparticulate matrix. A PDI close to 0.2 indicates a relatively narrow distribution suitable for experimental nanodelivery studies (Mehrotra et al., 2024; Sultan et al., 2022; Ukwubile et al., 2025a). VALE-CSNPs possessed a zeta potential of +31.6 mV. The positive surface charge is consistent with protonated amino groups in chitosan. Although zeta potential cannot independently predict biological stability, the magnitude of the measured charge suggests appreciable electrostatic repulsion among particles under the measurement conditions. The positive surface characteristics of chitosan systems may additionally promote interaction with negatively charged biological membranes. The encapsulation efficiency of 84.7% indicates efficient association of VALE constituents with the chitosan-TPP matrix. Chitosan nanoparticles prepared through ionic gelation have been widely investigated because the process occurs under mild conditions and can be adapted for incorporation of diverse therapeutic payloads (Xue et al., 2024; Ahmad et al., 2023; Kumar et al., 2011). Contemporary literature continues to identify chitosan nanocarriers as promising platforms for controlled and cancer-directed delivery (Ahmad et al., 2023). The release study demonstrated sustained release of VALE over 48 h, with cumulative release of 76.4% at pH 7.4 compared with 92.3% at pH 5.5. The enhanced release at lower pH may reflect greater protonation and swelling of the chitosan matrix, thereby facilitating liberation of associated constituents. This observation supports pH-sensitive formulation behaviour (Herdiana et al., 2022; Moussa et al., 2025). However, acidic *in vitro* release should not be interpreted as evidence of tumor-specific targeting because the current formulation lacks a cancer-specific targeting ligand and was not evaluated for tumor biodistribution. A major observation was the reduction in the MCF-7 IC_{50} from 84.6 µg/mL for free VALE to 31.8 µg/mL following nanoencapsulation, corresponding to an approximately 2.66-fold enhancement in apparent cytotoxic potency. Previous studies have independently demonstrated that *V. amygdalina* extracts reduce MCF-7 viability and can induce concentration- and time-dependent cell death (Pruthvish et al., 2021). The present findings extend this pharmacological concept by indicating that incorporation into a chitosan nanocarrier can substantially increase the apparent activity of the extract. Several factors could contribute to this effect. Encapsulation may improve dispersion of poorly water-soluble phytochemicals, protect labile constituents from degradation, and increase nanoparticle-cell interactions (Xue et al., 2024). Nevertheless, these explanations remain hypotheses because nanoparticle uptake was not directly quantified in the present study. Fluorescently labelled nanoparticle uptake, confocal microscopy, or quantitative intracellular chemical analysis would be required to demonstrate enhanced cellular internalization directly. The inclusion of MCF-10A cells provides an important distinction between increased potency and increased selectivity. Free VALE produced an SI of 2.08, whereas VALE-CSNPs produced an SI of 4.33. Thus, despite some increase in activity against non-tumorigenic mammary cells, the increase in activity against MCF-7 cells was substantially greater. The approximately two-fold improvement in SI suggests that nanoencapsulation did not simply increase nonspecific cytotoxicity. Annexin V-FITC/PI analysis provided further evidence regarding the nature of cell death. Free VALE resulted in 32.9% total apoptosis, whereas VALE-CSNPs increased total apoptosis to 61.5%. Importantly, necrosis accounted for only 4.4% of the VALE-CSNP-treated population, suggesting that the marked reduction in viable cells was predominantly associated with apoptotic rather than acute necrotic death. This finding agrees broadly with previous observations that *V. amygdalina* induces Annexin V-positive apoptosis in MCF-7 cells. Earlier mechanistic investigations have also implicated both intrinsic and extrinsic apoptotic processes and alterations in Bcl-2-family proteins following exposure of breast cancer cells to *V. amygdalina* extract. The molecular results further supported a shift toward apoptosis. Bax increased 2.91-fold following VALE-CSNP treatment, whereas Bcl-2 decreased to 0.34-fold of control. The resulting increase in the Bax/Bcl-2 balance is consistent with promotion of mitochondrial apoptotic signalling. Caspase-7 activity concurrently increased 3.26-fold. Caspase-7 was deliberately selected rather than caspase-3 because the widely used MCF-7 cell line is deficient in functional caspase-3 as a consequence of a deletion affecting the *CASP3* gene. Reporting caspase-3 activation in unmodified MCF-7 cells without verification can therefore lead to erroneous mechanistic conclusions. Caspase-7 provides a more defensible executioner-caspase endpoint in this experimental context. The combined increase in Annexin V-positive cells, elevation of Bax, suppression of Bcl-2 and activation of caspase-7 strongly supports an association between VALE-CSNP exposure and enhanced apoptotic signalling. However, these data establish an association rather than definitive molecular causality. Demonstration that Bax/Bcl-2 modulation or caspase-7 activation is required for VALE-CSNP-induced cell death would require knockdown, inhibition, or rescue experiments. Some limitations should be considered. First, the study employed a single malignant cell line. Breast cancer is molecularly

heterogeneous, and findings in MCF-7 cells cannot automatically be generalized to HER2-positive or triple-negative breast cancer. Future studies should include additional breast cancer cell lines such as MDA-MB-231 and SK-BR-3. Second, VALE represents a chemically complex botanical extract. Although LC-MS profiling provides chemical characterization, the contribution of individual constituents to the observed activity remains unknown. Bioassay-guided fractionation and testing of isolated compounds would help identify the principal active constituents. Third, intracellular nanoparticle uptake was not directly measured. Fourth, the present experiments do not establish pharmacokinetics, biodistribution, systemic safety, or *in vivo* antitumor efficacy. Finally, physicochemical stability during extended storage requires further investigation before pharmaceutical development. Despite these limitations, the study demonstrates a coherent relationship between nanoparticle formulation, improved apparent cytotoxic potency, greater cancer-cell selectivity, and enhanced apoptosis. These findings provide a rationale for further investigation of *V. amygdalina*-loaded chitosan nanoparticles as a natural-product nano pharmaceutical platform.

Conclusion

Vernonia amygdalina leaf extract was successfully incorporated into chitosan nanoparticles using ionic gelation. The optimized formulation had a mean particle size of 168.4 ± 8.7 nm, PDI of 0.226 ± 0.031, positive zeta potential of +31.6 ± 2.1 mV, and encapsulation efficiency of 84.7 ± 3.2%. Nanoencapsulation reduced the MCF-7 IC_{50} from 84.6 ± 5.1 to 31.8 ± 2.7 µg/mL and increased the selectivity index from 2.08 to 4.33. VALE-CSNPs also increased total apoptosis to 61.5%, accompanied by increased Bax expression, reduced Bcl-2 expression, and increased caspase-7 activity. These findings indicate that chitosan nanoparticle-mediated delivery enhances the apparent anticancer activity and selectivity of *V. amygdalina* leaf extract in MCF-7 cells and that the enhanced response is associated with increased apoptotic signalling. Further studies involving additional breast cancer models, nanoparticle-uptake experiments, active-compound standardization and *in vivo* efficacy, pharmacokinetic and safety investigations are warranted.

Acknowledgement

The authors are grateful to Mr. Yusuf Babagana of the Department of Pharmacology and Toxicology for his technical assistance in this work.

Author contributions

C.A.U. conceived and designed the study, developed the methodology, nanoparticle formulation and characterization, supervised the research, contributed to data analysis and interpretation, and drafted the original manuscript. **T.S.M.** contributed to the experimental investigations, data acquisition, analysis of the results, and review and editing. **M.Y.D.** contributed to the phytochemical and biological investigations, data analysis and interpretation, and manuscript review. All authors critically reviewed and revised the manuscript, approved the final version for publication, and agreed to be accountable for the integrity of the work.

Funding

This research received no specific grant from any funding agency in the public, commercial, or not-for-profit sectors.

Competing interest

The authors declare that they have no competing interests.

Ethics approval

The study involved established human cell lines and did not involve direct recruitment of human participants or experimental animals; therefore, no ethical approval is required. However, laboratory ethics were observed in the study involving cell lines.

AI tool usage declaration

The authors declare that they used AI-assisted tools solely for language editing, grammatical correction, and improving the manuscript's clarity and readability. No AI tools were used to generate research data, analyze results, interpret findings, or develop the scientific content of the manuscript.

References

Acuña-Pilarte, K., & Koh, M. Y. (2025). The HIF axes in cancer: Angiogenesis, metabolism, and immune-modulation. *Trends in Biochemical Sciences, 50*(8), 677–694. https://doi.org/10.1016/j.tibs.2025.06.005

Adams, I., Adi-Dako, O., Appiah-Opong, R., Ofori-Attah, E., Aning, A., Ofori, E. K., Nyankson, E., & Amponsah, S. K. (2025). In vitro anticancer activities of curcumin-loaded copper oxide–halloysite nanotubes composite. *Journal of Nanotechnology, 2025*(1). https://doi.org/10.1155/jnt/7535486

Ahmad, N., Khan, M. R., Palanisamy, S., & Mohandoss, S. (2023). Anticancer drug-loaded chitosan nanoparticles for in vitro release, promoting antibacterial and anticancer activities. *Polymers, 15*(19), 3925. https://doi.org/10.3390/polym15193925

Akinduti, P. A., Emoh-Robinson, V., Obamoh-Triumphant, H. F., Obafemi, Y. D., & Banjo, T. T. (2022). Antibacterial activities of plant leaf extracts against multi-antibiotic-resistant *Staphylococcus aureus* associated with skin and soft tissue infections. *BMC Complementary Medicine and Therapies, 22*(1), 1–11. https://doi.org/10.1186/s12906-022-03527-y

Alfuraydi, A. A., Aziz, I. M., & Almajhdi, F. N. (2024). Assessment of antioxidant, anticancer, and antibacterial activities of the rhizome of ginger (*Zingiber officinale*). *Journal of King Saud University - Science, 36*(3), 103112. https://doi.org/10.1016/j.jksus.2024.103112

Almudhafar, S. M. A., & Al-Hamdani, M. A. (2022). Antibacterial and anticancer effects of silver nanoparticles synthesised using *Eragrostis tef* and *Vitellaria paradoxa* seeds extract. *Basrah Journal of Agricultural Sciences, 35*(2), 132–159. https://doi.org/10.37077/25200860.2022.35.2.10

Awadh, A. I., Ajeed, A. M., Khadir, F. K., & Abdulamir, H. A. (2024). Vascular endothelial growth factor (VEGF) and its role in the progression and development of breast tumor. *International Journal of Pharmaceutical and Bio-Medical Science, 4*(4), 407–415. https://doi.org/10.47191/ijpbms/v4-i4-23

Cartwright, I. M., Liu, X., Zhou, M., Li, F., & Li, C. Y. (2017). Essential roles of caspase-3 in facilitating MYC-induced genetic instability and carcinogenesis. *eLife, 6*, 1–14. https://doi.org/10.7554/eLife.26371

Fakudze, N., Sarbadhikary, P., Abrahamse, H., & George, B. P. (2026). Enhanced anticancer potential of *Punica granatum* fruit extract in combination with pheophorbide-a mediated photodynamic therapy on MCF-7 breast cancer cells. *Advances in Traditional Medicine, 26*(1), 143–161. https://doi.org/10.1007/s13596-025-00840-y

Faujdar, S., Sati, B., Sharma, S., Pathak, A. K., & Paliwal, S. K. (2019). Phytochemical evaluation and anti-hemorrhoidal activity of bark of *Acacia ferruginea* DC. *Journal of Traditional and Complementary Medicine, 9*(2), 85–89. https://doi.org/10.1016/j.jtcme.2018.02.003

Ghannam, H. E., Talab, A. S., Dolgano, N. V., Husse, A. M. S., & Abdelmagui, N. M. (2016). Characterization of chitosan extracted from different crustacean shell wastes. *Journal of Applied Sciences, 16*(10), 454–461. https://doi.org/10.3923/jas.2016.454.461

Herdiana, Y., Wathoni, N., Shamsuddin, S., & Muchtaridi, M. (2022). Drug release study of the chitosan-based nanoparticles. *Heliyon, 8*(1), e08674. https://doi.org/10.1016/j.heliyon.2021.e08674

Ikpefan, E. O., Ukwubile, C. A., Omeje, E. O., Ovbiagele, S. O., Mudassar, A., & Shah, Z. A. (2024). Phytosterols and diterpenoids isolated from *Euphorbia graminea* Jacq. (Asteraceae) leaves exhibit antiproliferative effects against human MCF-7 breast and NCI-H460 lung cancer cell lines. *Nigerian Journal of Pharmaceutical and Biomedical Research, 8*(1), 11–30.

Joseph, A., Dhanraj, K., Ramalingam, S., & Saravanan, R. (2018). Treating cervical cancer with herbs: A review. *Asian Journal of Pharmaceutical and Clinical Research, 11*(7), 4–10. https://doi.org/10.22159/ajpcr.2018.v11i7.25580

Khanmohammadi, M., Elmizadeh, H., & Ghasemi, K. (2015). Investigation of size and morphology of chitosan nanoparticles used in drug delivery system employing chemometric technique. *Iranian Journal of Pharmaceutical Research, 14*(3), 665–675. https://doi.org/10.22037/ijpr.2015.1761

Kumar, D. A., Dharmendra, S., Jhansee, M., Shrikant, N., & Pandey, S. P. (2011). Development and characterization of chitosan nanoparticles loaded with amoxicillin. *International Research Journal of Pharmacy, 2*, 145–151.

Mehrotra, S., Goyal, V., Dimkpa, C. O., & Chhokar, V. (2024). Green synthesis and characterization of ginger-derived silver nanoparticles and evaluation of their antioxidant, antibacterial, and anticancer activities. *Plants, 13*(9), 1255. https://doi.org/10.3390/plants13091255

Moldovan, R. I., Oprean, R., Benedec, D., Hanganu, D., Duma, M., Oniga, I., & Vlase, L. (2014). LC-MS analysis, antioxidant and antimicrobial activities for five species of *Mentha* cultivated in Romania. *Digest Journal of Nanomaterials and Biostructures, 9*(2), 559–566.

Moussa, A. K., Abd El-Rahman, H. A., Mohamed, R. R., & Hanna, D. H. (2025). Hyaluronic acid-based pH-sensitive nanogel: Synthesis, characterization, and assessment for acyclovir delivery in vitro and in vivo. *Biomacromolecules, 26*(1), 341–362. https://doi.org/10.1021/acs.biomac.4c01189

Ndidi, C., Ngozika, F., Amaka, P., & Blessing, N. (2020). Phytochemical and antibacterial activities of *Vernonia amygdalina* leaves (bitter leaf) on two drug-resistant bacteria. *International Journal of Research Studies in Microbiology and Biotechnology, 7*(5), 59–66. https://doi.org/10.20431/2454-9428.0601004

Nelson, V. K., Sahoo, N. K., Sahu, M., Sudhan, H. H., Pullaiah, C. P., & Muralikrishna, K. S. (2020). In vitro anticancer activity of *Eclipta alba* whole plant extract on colon cancer cell HCT-116. *BMC Complementary Medicine and Therapies, 20*, 355. https://doi.org/10.1186/s12906-020-03118-9

Pal, A., Sanyal, S., Das, S., & Sengupta, T. K. (2024). Effect of *Lantana camara* ethanolic leaf extract on survival and migration of MDA-MB-231 triple-negative breast cancer cell line. *Journal of Herbal Medicine, 43*, 100837. https://doi.org/10.1016/j.hermed.2023.100837

Pidgeon, G. P., Barr, M. P., Harmey, J. H., Foley, D. A., & Bouchier-Hayes, D. J. (2001). Vascular endothelial growth factor (VEGF) upregulates BCL-2 and inhibits apoptosis in human and murine mammary adenocarcinoma cells. *British Journal of Cancer, 85*(2), 273–278. https://doi.org/10.1054/bjoc.2001.1876

Pruthvish, R., Gopinath, S. M., Sushma, P., Anisha, S., Shiva, J., Prasad, J. S. K., & Shivmallu, C. (2021). In-silico evaluation of anti-cancerous activity of herbal plant extracts. *Bulletin of Environment, Pharmacology and Life Sciences, 10*(4), 105–117.

Saneja, A., Sharma, L., Dubey, R. D., Mintoo, M. J., Singh, A., Kumar, A., Sangwan, P. L., Tasaduq, S. A., Singh, G., Mondhe, D. M., & Gupta, P. N. (2017). Synthesis, characterization and augmented anticancer potential of PEG-betulinic acid conjugate. *Materials Science and Engineering: C, 73*, 616–626. https://doi.org/10.1016/j.msec.2016.12.109

Sayed, A. A., Abdel Moteleb, M. M., El Shafee, E., & Hanna, D. H. (2024). Oral drug delivery vehicle for insulin and curcumin based on egg albumin-dextran conjugate: In vitro and in vivo studies. *Journal of Drug Delivery Science and Technology, 100*, 106052. https://doi.org/10.1016/j.jddst.2024.106052

Shehzadi, S., Noreen, S., Imran, H., Ikram, A., Arshad, M. T., & Gnedeka, K. T. (2025a). Unveiling the phytochemical profile and anti-cancer potential of *Lantana camara* leaf and root extracts against MCF-7, HepG2, and A549 cancer cell lines. *Food Science & Nutrition, 13*(9), e70915. https://doi.org/10.1002/fsn3.70915

Shehzadi, S., Noreen, S., Imran, H., Ikram, A., Arshad, M. T., & Gnedeka, K. T. (2025b). Unveiling the Phytochemical Profile and Anti-Cancer Potential of Lantana camara Leaf and Root Extracts Against MCF-7, HepG2, and A549 Cancer Cell Lines. Food Science and Nutrition, 13(9), 1–13. https://doi.org/10.1002/fsn3.70915

Subramaniyan, N. K., Elumalai, K., Rajangam, J., Palei, N. N., Talari, D., Balaji, A., & Surendran, V. (2023). Protective role of *Vernonia cinerea* against the carmoisine-induced brain injury and anxiogenic effect in mice. *Egyptian Journal of Basic and Applied Sciences, 10*(1), 12–24. https://doi.org/10.1080/2314808X.2022.2122289

Sudu Dewage, M. A. R., Lorensu Hewage, V. C., George, G. D. N., & Weerasinghe, W. (2026). Phytochemical screening, in vitro and in silico evaluation of antioxidant, anti-diabetic, antibacterial activities of rhizome extracts from *Rhinacanthus nasutus* (L.) Kurz (snake jasmine). *In Silico Pharmacology, 14*(2), 203. https://doi.org/10.1007/s40203-026-00708-2

Sultan, M. H., Moni, S. S., Madkhali, O. A., Bakkari, M. A., Alshahrani, S., Alqahtani, S. S., Alhakamy, N. A., Mohan, S., Ghazwani, M., Bukhary, H. A., Almoshari, Y., Salawi, A., & Alshamrani, M. (2022). Characterization of cisplatin-loaded chitosan nanoparticles and rituximab-linked surfaces as target-specific injectable nano-formulations for combating cancer. *Scientific Reports, 12*(1), 1–16. https://doi.org/10.1038/s41598-021-04427-w

Ukwubile, C. A. (2017). Preliminary phytochemical screening and antibacterial activity of *Thaumatococcus daniellii* (Benn.) Benth. (Marantaceae) leaf extract. *Journal of Bacteriology & Mycology: Open Access, 4*(2), 2–6. https://doi.org/10.15406/jbmoa.2017.04.00086

Ukwubile, C. A., Yesufu, H. B., Okoro, R. N., Ahuchaogu, A. A., Umeokoli, B. O., Agu, M. O., Menkiti, N. D., & Ida, P. A. (2025a). Chitosan-encapsulated linoleic acid from *Leucaena leucocephala* (Lam.) de Wit. inhibits FOXL2 mutation in MNU-induced ovarian granulosa cell tumors in Wistar rats. *Next Nanotechnology, 8*, 100191. https://doi.org/10.1016/j.nxnano.2025.100191

Ukwubile, C. A., Nuhu, A., Famurewa, A. C., Nettey, H., & Odugu, J. A. (2025b). Chitosan nanoparticles encapsulating *Ipomoea digitata* L. tuber and *Jatropha gossypiifolia* L. leaf extract suppress NF-κB, Wnt/β-catenin, and MAPK signaling pathways in HCT116 and SW480 colorectal cancer cells. *International Journal of Advanced Multidisciplinary Research Studies, 5*, 45–58. https://doi.org/10.62225/2583049x.2025.5.5.4860

Vaezifar, S., Razavi, S., Golozar, M. A., Karbasi, S., Morshed, M., & Kamali, M. (2013). Effects of some parameters on particle size distribution of chitosan nanoparticles prepared by ionic gelation method. *Journal of Cluster Science, 24*(3), 891–903. https://doi.org/10.1007/s10876-013-0583-2

Xue, Y., Ruan, Y., Wang, Y., Xiao, P., & Xu, J. (2024). Signaling pathways in liver cancer: Pathogenesis and targeted therapy. *Molecular Biomedicine, 5*(1), 20. https://doi.org/10.1186/s43556-024-00184-0